ELSEVIER

Journal of Crystal Growth 220 (2000) 384–392

JOURNAL OF CRYSTAL GROWTH

www.elsevier.nl/locate/jcrysgro

Surface reconstruction phase diagrams for InAs, AlSb, and GaSb

A.S. Bracker*, M.J. Yang, B.R. Bennett, J.C. Culbertson, W.J. Moore

Electronics Science and Technology Division, Naval Research Laboratory, Code 6876, 4555 Overlook Avenue, SW, Washington, DC 20375-5347, USA

Received 19 July 2000; accepted 15 September 2000
Communicated by A.Y. Cho

Abstract

We present experimental flux-temperature phase diagrams for surface reconstruction transitions on the 6.1 Å compound semiconductors. The phase transitions occur within or near typical substrate temperature ranges for growth of these materials by molecular beam epitaxy and therefore provide a convenient temperature standard for optimizing growth conditions. Phase boundaries for InAs (0 0 1) $[(2\times4)\rightarrow(4\times2)]$, AlSb (0 0 1) $[c(4\times4)\rightarrow(1\times3)]$, and GaSb (0 0 1) $[(2\times5)\rightarrow(1\times3)]$ are presented as a function of substrate temperature and Group V-limited growth rate (proportional to flux), for both cracked and uncracked Group V species. We discuss differences between materials in the slopes and offsets of the phase boundaries for both types of Group V species.

PACS: 18.15.Hi; 81.05.Ea; 68.35.Bs; 68.35.Rh

Keywords: Molecular beam epitaxy; Gallium antimonide; Aluminum antimonide; Indium arsenide; Surface reconstruction

1. Introduction

The compound semiconductors with 6.1 Å lattice constant, including InAs, GaSb, and AlSb, have received increasing attention in recent years because of their potential for electronic and optical device applications [1–6]. A unique combination of band offset (broken gap type II, between InAs and GaSb), high InAs electron mobility, and InAs surface Fermi level pinning permit novel device designs and improved performance that are difficult to achieve with other compound semiconductors. In order to realize these benefits, epitaxial growth and device processing technologies for the 6.1 Å compound semiconductors must advance to the level of more mature material systems such as GaAs/AlGaAs and InP/InGaAs.

In order to grow the highest quality compound semiconductor thin films by molecular beam epitaxy (MBE), precursor fluxes and substrate temperature should be optimized [7,8]. These growth parameters affect the rates of adsorption, desorption, and surface diffusion of Group III and V species, and therefore influence the quality of crystal growth. Activation barriers and preexponentials

* Corresponding author. Fax: + 1-202-767-1165.
E-mail address: bracker@bloch.nrl.navy.mil (A.S. Bracker).

0022-0248/00/$ - see front matter
PII: S0022-0248(00)00871-X

Report Documentation Page

Form Approved
OMB No. 0704-0188

1. REPORT DATE	2. REPORT TYPE	3. DATES COVERED
JUL 2000		**00-00-2000 to 00-00-2000**

4. TITLE AND SUBTITLE	5a. CONTRACT NUMBER
Surface reconstruction phase diagrams for InAs, AlSb, and GaSb	5b. GRANT NUMBER
	5c. PROGRAM ELEMENT NUMBER
6. AUTHOR(S)	5d. PROJECT NUMBER
	5e. TASK NUMBER
	5f. WORK UNIT NUMBER
7. PERFORMING ORGANIZATION NAME(S) AND ADDRESS(ES) **Naval Research Laboratory,Electronics Science and Technology Division,4555 Overlook Avenue SW,Washington,DC,20375**	8. PERFORMING ORGANIZATION REPORT NUMBER
9. SPONSORING/MONITORING AGENCY NAME(S) AND ADDRESS(ES)	10. SPONSOR/MONITOR'S ACRONYM(S)
	11. SPONSOR/MONITOR'S REPORT NUMBER(S)

12. DISTRIBUTION/AVAILABILITY STATEMENT
Approved for public release; distribution unlimited

13. SUPPLEMENTARY NOTES

14. ABSTRACT
see report

15. SUBJECT TERMS

16. SECURITY CLASSIFICATION OF:			17. LIMITATION OF ABSTRACT	18. NUMBER OF PAGES	19a. NAME OF RESPONSIBLE PERSON
a. REPORT **unclassified**	b. ABSTRACT **unclassified**	c. THIS PAGE **unclassified**	**Same as Report (SAR)**	**9**	

for these processes depend on the structure and stoichiometry of the material surface (see e.g. Refs. [9,10]), which are in turn affected by temperature and beam flux. To achieve the best growth conditions, it is therefore desirable to know the reconstruction phase boundaries over typical beam flux and substrate temperature ranges.

The flux-temperature phase diagram is also convenient for estimating substrate temperature, particularly, when standard techniques for temperature measurement are unavailable. Remote thermocouple measurements in vacuum are notoriously inaccurate. Furthermore, their calibration can change during growth of small-bandgap epilayers (e.g. InAs and GaSb), due to radiative heating that increases with film thickness [11,12]. The accuracy of optical pyrometry is limited by stray light from the substrate heater or source ovens, coating of the viewport, changes in substrate emissivity, and limited sensitivity below 500°C [13]. Transmission thermometry, which monitors the shift in the optical transmission edge of the substrate, is an effective alternative to pyrometry [14–16]. However, this technique is not possible for InAs substrates due to free electron absorption, and measurements for 6.1 Å heteroepitaxy on GaAs substrates are not possible when a small-bandgap epilayer is thick enough to absorb most of the source light ($>1\,\mu m$). When these or other techniques are not available, observation of known surface reconstruction transitions remains a convenient means to estimate substrate temperatures.

There have been several reports of reconstruction phase diagrams for III–V materials, especially for GaAs. Early work on reconstruction transitions [17,18] includes measurements for all zincblende III–V compounds at a fixed Group V flux [18]. Full phase diagrams have been reported for GaAs (0 0 1) [19–23], GaAs (1 1 1) [24], AlAs (0 0 1) [19,20,25], AlGaAs (0 0 1) [22], and for the 6.1 Å materials [16,23,26,27], although not all with calibrated fluxes of both cracked and uncracked Group V species. Recent results on GaSb from our group were presented previously [16] and are discussed in this work as well.

Phase diagrams typically describe thermodynamic equilibrium conditions. However, for MBE conditions during surface stabilization by a Group V flux, the system is not in strict equilibrium: the vapor and solid phases are at different temperatures; the vapor velocity distribution is anisotropic; the incident and desorbing species may not be the same. Nevertheless, equilibrium thermodynamics may be used as an approximate description of a Group V-stabilized surface [7,8]. We adopt this view, although in Section 4 we discuss some evidence for non-equilibrium behavior.

2. Experimental method

The 6.1 Å semiconductors studied in this report were grown by solid-source MBE. Growth rates and surface reconstruction symmetry were monitored with reflection high-energy electron diffraction (RHEED). A 10 kV electron beam was incident on the sample surface between 1.5° and 2.5°. The beam had been previously adjusted to focus on the RHEED phosphor screen (~ 70 cm from electron gun to screen) without the sample in place. All three 6.1 Å materials were grown on semi-insulating GaAs (0 0 1) substrates, and the GaSb measurement was also repeated on GaSb substrates, producing no shift of the phase boundary [16]. AlSb and GaSb layers on GaAs were roughly 1 μm thick, while InAs was grown on a 1 μm AlSb buffer. Thin layers of InAs (1000 Å) were used in order to minimize absorption of radiation from the substrate heater, which is needed for transmission thermometry. In order to confirm that strain in the thin InAs layer (1.3% lattice mismatch with AlSb) does not significantly influence the reconstruction transition temperature, we measured this temperature for InAs (0 0 1) $[(2\times4)\rightarrow(4\times2)]$ under a background arsenic flux for thickness up to 8000 Å. No dependence on the InAs layer thickness was observed.

Substrate temperatures were measured by transmission thermometry. This technique relies on the change in the substrate bandgap with temperature [14–16]. Briefly, light from the substrate heater is partially transmitted through the substrate and exits the chamber through a viewport. The light is chopped (for phase-sensitive detection), focused into an optical fiber, dispersed by a grating

spectrometer, and finally detected with a photodiode. The transmission spectrum of the substrate is obtained by taking the ratio of the spectrum obtained with the substrate in place to a background spectrum of the bare substrate heater emission. For GaSb substrates, the relation between transmission edge and substrate temperature was taken from Ref. [16]. In the appendix, we present a new calibration for GaAs substrates, in order to update deficiencies in an earlier version.

EPI cracker models 500V-As and 175-Sb were used to produce cracked Group V species. By choosing the appropriate operating conditions for the arsenic source, it is straightforward to produce either arsenic dimers (As_2) or tetramers (As_4), but the antimony cracker source (cracker temperature 900°C) produces a mixture of Sb_2 and Sb atoms due to the small Sb_2 bond strength. A detailed characterization (using the 175-Sb) was reported in Ref. [28] and showed that the source produces a large flux-dependent proportion of Sb atoms under operating conditions typical for our work. Antimony dimer beams discussed in later sections of this paper should therefore be understood to include atoms as well. We use a separate antimony source (operating temperatures $<500°C$) to produce tetramers.

Although molecular beam fluxes are commonly reported as ion gauge pressure readings, such readings are often not reproducible between laboratories due to differences in ion gauge geometry, electrode voltages, filament and electrode coatings, etc. Furthermore, the conversion from an ion gauge reading to beam fluxes requires quantitative values for the species-dependent ionization cross-sections. Because of these shortcomings, we also present phase diagrams with the flux expressed in units of growth rate at a III/V flux ratio for which the Group V flux is limiting. This approach has been used previously in studies of epitaxial growth and surface reconstructions on GaAs (see e.g. Refs. [16,29]).

We used the following procedure to convert to Group V-limited growth rate units. These measurements are made separately from the phase transition measurements. For a fixed Group V flux, the growth rate is measured from RHEED oscillations as a function of Group III cell temperatures.

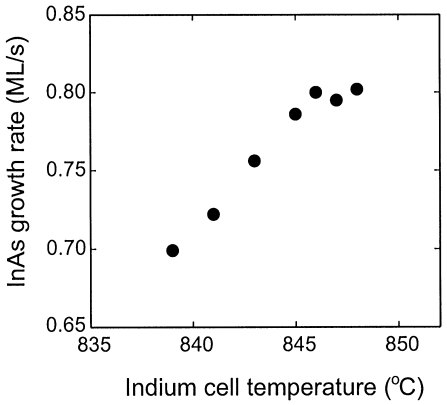

Fig. 1. Typical Group V-limited growth rate measurement, here for InAs with As_2 (3.2×10^{-6} Torr beam equivalent pressure). Arsenic flux limits growth at 0.802 ML/s, yielding $g_2 = 4.0\times10^{-6}$ Torr/(ML/s).

As the Group III flux is increased, the growth rate eventually saturates as growth becomes limited by the Group V flux. An example of this behavior is shown in Fig. 1 for InAs. Dividing the Group V flux (beam-equivalent pressure units, torr) by the saturation growth rate (ML/s) gives the values g_2 (for dimers) and g_4 (for tetramers) that are used to rescale the vertical axes of the phase diagrams. A Group III-rich reconstruction RHEED pattern is often observed during the V-limited growth oscillations. We found that g_2 and g_4 were independent of Group V flux, with the only exception at the lowest fluxes of arsenic, where non-beam arsenic species may contribute a significant fraction to the ion gauge reading. The calibration was carried out at 420°C, 430°C, and 520°C for InAs, GaSb, and AlSb, respectively. These temperatures should be roughly reproduced when repeating the calibration, because the Group V incorporation coefficients during growth on (0 0 1) surfaces begin to decrease at higher substrate temperature (see e.g. Refs. [29,30][1] for typical behavior).

[1] The InAs phase diagram in Ref. [23] for the $(2\times4)\rightarrow(4\times2)$ transition during growth should correspond roughly to the temperature dependence of V-limited growth as defined by g_x in this work.

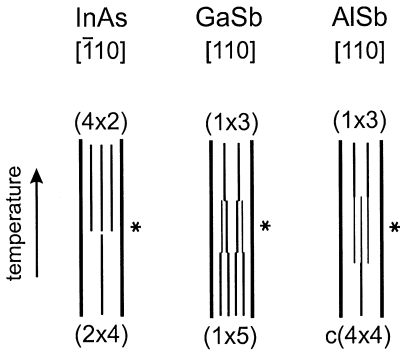

Fig. 2. Schematic representation of RHEED pattern evolution as substrate temperature is ramped through phase transitions. Stars mark the points chosen as empirical definitions of the phase transitions.

3. Phase diagrams

Our experimental definitions for the reconstruction phase transitions are based on changes in the RHEED pattern (Fig. 2). Our primary intention in choosing these definitions was that the measurements could be reproduced in other laboratories. We are not concerned with whether the corresponding changes in surface structure satisfy more rigorous criteria for a phase transition. Changes in surface periodicity occur at different temperatures for different crystal directions, and mixed phases or domains may exist around the transition temperature. We simply represent the transition region as a line, while recognizing that additional surface structures may exist.

Several sources of experimental error contribute to uncertainty in the phase transition temperatures. The two most important errors in our experience were the position of the RHEED electron beam on the substrate (due to lateral temperature gradients) and unsteady ramp rates. A background pressure of undesired Group V species is likely to shift the transition temperature, especially for antimonides when arsenic is a background species. We kept the arsenic source at idle temperature during antimonide measurements, and vice versa, but unfortunately this may not be possible during heterostructure growths that require both Group V species. Finally, there is some subjectivity in judging changes in diffraction streaks as described in Fig. 2. Given these errors, repeated measurements rarely varied by more than 10°C.

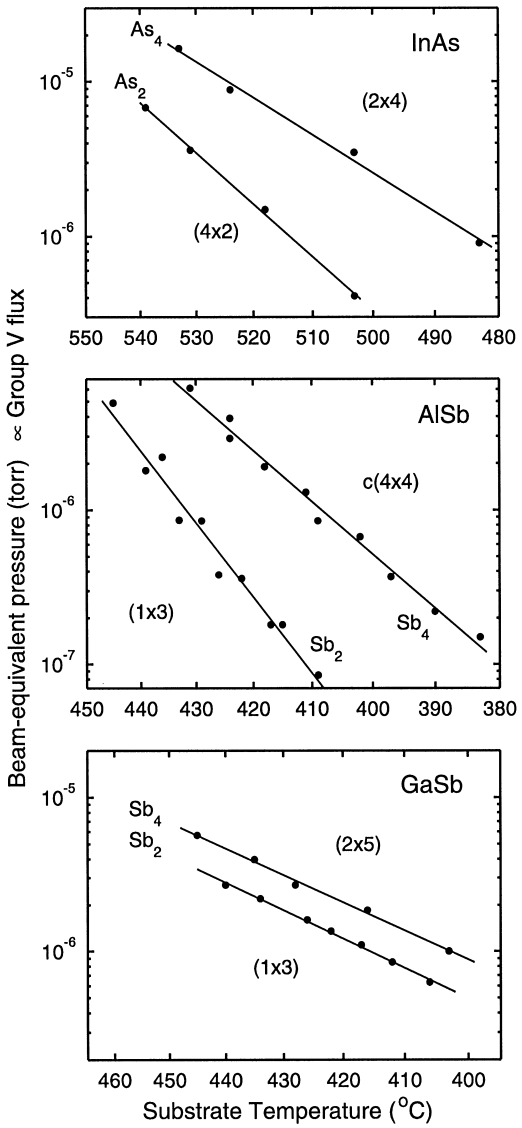

Fig. 3. Reconstruction phase diagrams, with Group V flux expressed in beam-equivalent pressure units (s_2 and s_4 in Torr). Horizontal axis is linear in reciprocal absolute temperature. Solid lines are fits using the expression and parameters in Table 1.

Figs. 3 and 4 show the phase diagrams for surface reconstructions on InAs, GaSb, and AlSb. We used a simple exponential form to fit the data points, as described in Table 1. The vertical axes of Fig. 3 are

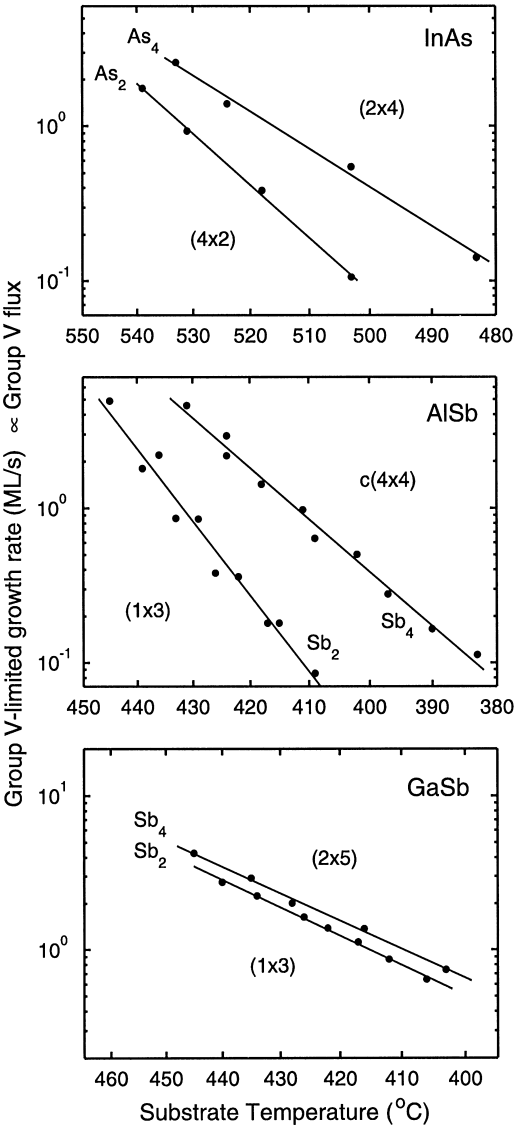

Fig. 4. Reconstruction phase diagrams, with Group V flux expressed in units of Group V-limited growth rate (s_2/g_2 and s_4/g_4 in ML/s). Horizontal axis is linear in reciprocal absolute temperature. Solid lines are fits using the expression and parameters in Table 1.

expressed in the units of beam-equivalent pressure (Torr) as measured with an ion gauge, which is proportional to the absolute Group V atomic flux required to stabilize the surface at the phase boundary. The plots on this scale are referred to subsequently as s_2 and s_4, for *stabilization* under

Table 1
Parameters used in the expression flux $= \exp(-E/k_B T + B)$ for fits in Figs. 3 and 4. B_{Torr} and $B_{ML/s}$ give flux in units of beam-equivalent pressure (Torr) and Group V-limited growth rate (ML/s), respectively

		E (eV)	B_{Torr}	$B_{ML/s}$
InAs	As_2	4.16	47.5	60.0
	As_4	2.95	31.5	43.5
AlSb	Sb_2	4.64	62.6	76.4
	Sb_4	3.10	39.0	52.5
GaSb	Sb_2	1.78	16.3	30.1
	Sb_4	1.72	15.7	29.2

a Group V flux of dimers or tetramers, respectively. This form of the phase diagram may be used as a quick reference for estimating substrate temperature, but these values may not compare well between laboratories, for the reasons discussed earlier.

Fig. 4 shows the phase diagrams with vertical axes rescaled in units of V-limited growth rate (s_2/g_2 and s_4/g_4). The divisors g_2 and g_4 (for *growth* with dimers and tetramers, respectively) are proportional to the incident Group V flux (Torr) during V-limited growth divided by the Group V-limited growth rate in ML/s. They are $g_2(\mathrm{AlSb}) = 1.0\times10^{-6}$, $g_4(\mathrm{AlSb}) = 1.3\times10^{-6}$, $g_2(\mathrm{GaSb}) = 1.0\times10^{-6}$, $g_4(\mathrm{GaSb}) = 1.3\times10^{-6}$, $g_2(\mathrm{InAs}) = 3.9\times10^{-6}$, $g_4(\mathrm{InAs}) = 6.4\times10^{-6}$, with units of Torr/(ML/s). The units s_x/g_x are still proportional to the incident Group V flux required for stabilization, but they are more easily transferred between laboratories than s_x, because ion gauge sensitivities are divided out.[2] We stress that g_x was measured separately and at only one substrate temperature for purposes of rescaling each phase

[2] When g_x and s_x are both measured in the temperature range where g_x is independent of temperature, then the units s_x/g_x are also equal to the rate at which Group V atoms would be incorporated into the crystal during a V-limited growth measurement for flux s_x. This condition is approximately true for GaSb and AlSb. However for InAs, the reconstruction phase boundaries were measured at temperatures far higher than where g_x was measured and in a range where g_x rises rapidly with temperature.

boundary in Fig. 3 to produce Fig. 4. No growth occurred during the phase transition measurements. The slopes of the phase boundaries reflect the thermodynamics and kinetics of stabilization only.

The changes in the RHEED pattern used to identify the phase transitions are marked by stars in Fig. 2. For all measurements, the substrate temperature was ramped upward at a rate of 2° per minute. For AlSb (0 0 1) [$c(4\times4)\rightarrow(1\times3)$],[3] we defined the transition temperature by equal intensities for the 1/3 and 2/3 streaks of the $3\times$ pattern and the 1/2 streak of the $2\times$ pattern [from $c(4\times4)$], in the [1 1 0] direction.

The InAs (0 0 1) [$(2\times4)\rightarrow(4\times2)$] transition was defined as the first appearance of the $4\times$ diffraction streaks in the [$\bar{1}$ 1 0] direction. Yamaguchi and Horikoshi have also studied this transition in detail for As_4 flux [26]. They used a specialized apparatus to monitor changes in the RHEED specular intensity and measured temperature and pressure with pyrometry and an ion gauge, respectively. Their measured phase boundary for As_2 flux occurred roughly 30°C lower than ours, with flux expressed as an ion gauge reading. This discrepancy is probably a consequence of a different experimental definition for the transition, and possibly also due to inaccuracies associated with pyrometer or ion gauge measurements.

The GaSb [$(2\times5)\rightarrow(1\times3)$] phase diagram was recently reported by our group [16].[4] The phase diagram from that work is reproduced here in Figs. 3 and 4. The transition was defined by the appearance of a pseudo-(1×3) RHEED pattern, as the 1/5 and 4/5 streaks disappear, and before the 2/5 and 3/5 streaks move apart into the typical positions for the (1×3) pattern.

These definitions, combined with the experimental techniques described above for obtaining the flux scale in Fig. 4, should allow reproducible measurement of the phase boundaries in other laboratories. Because the phase boundaries fall in or near the usual growth temperature ranges for the 6.1 Å materials, they should prove useful for temperature calibration when other techniques are inaccurate or unavailable. Although the AlSb (0 0 1) [$c(4\times4)\rightarrow(1\times3)$] transition falls considerably below the optimal temperature range for AlSb growth (500–600°C), most device structures containing AlSb also contain InAs and GaSb, which are grown at temperatures below 500°C. The GaSb (0 0 1) [$(2\times5)\rightarrow(1\times3)$] transition falls within the common growth temperature range for InAs and GaSb (400–500°C), while the InAs (0 0 1) [$(2\times4)\rightarrow(4\times2)$] transition lies above this range.

We next discuss the significant differences between materials in the offsets and slopes of the phase boundaries for cracked and uncracked Group V species.

4. Reactivity of Group V dimers and tetramers

The reactivity of uncracked (tetramer) and cracked (dimer[5]) Group V species on III–V surfaces has long been an area of fundamental and practical interest. The form of the incoming species will affect the rates of adsorption, and quite possibly diffusion and desorption as well. Adsorption of gas phase Group V dimers may be as simple as a bond length change and rearrangement on the surface to form a surface dimer. In contrast, the tetrahedral Group V tetramers must undergo a more complicated electronic and nuclear rearrangement to produce surface dimers, resulting in slower rates. Some experimental results for gallium arsenide growth suggest that As_4 chemisorption requires the interaction of two neighboring physisorbed

[3] Recent work (Ref. [40]) has shown that the AlSb (1×3) is in fact a (4×3) structure, but the $4\times$ periodicity is usually not observed in RHEED.

[4] The GaSb "(2×5)" reconstruction discussed here appears in scanning tunneling microscope images as (2×10) or $c(2\times10)$ unit cells (see Ref. [41]). In RHEED, a (1×5) or (2×5) pattern is observed.

[5] For cracked antimony, this discussion assumes that the monomer content of the beam, which changes as a function of total flux, does not affect the antimony incorporation kinetics. Ref. [28] has shown that dimers and atoms have nearly identical incorporation probabilities during Group V-rich growth and proposed that this occurs because most antimony atoms rapidly form dimers on the surface.

tetramers [31,32], and ab initio cluster model results support this mechanism [33]. In this mechanism, two atoms from each tetramer are released to the gas phase, so that the incorporation coefficient is never larger than 50%. In contrast, 100% incorporation is possible with As_2. These stoichiometries have been widely assumed for III–V MBE growth since the early investigations of GaAs growth using modulated-beam mass spectrometry [31,34], however, other studies have reported As_4 incorporation coefficients greater than 50% [35–37]. Studies of antimonides report that Sb_4 incorporation coefficients are closer to 100% [38,39].

The vertical offsets between the dimer- and tetramer-phase boundaries in Fig. 4 (s_4/g_4 vs. s_2/g_2) reflect differences in the relative efficiency[6] of the two Group V species in stabilization vs. growth (s_4/s_2 vs. g_4/g_2).[7] For example, the GaSb phase boundaries for Sb_4 and Sb_2 are nearly coincident ($s_4/s_2 \approx g_4/g_2$), suggesting that fluxes of dimers and tetramers have roughly the same relative efficiencies in both stabilization and growth of GaSb. In contrast, the large offset between the AlSb phase boundaries implies that proportionally more Sb_4 is needed for stabilization than for growth ($s_4/s_2 > g_4/g_2$). Unless the different behaviors of AlSb and GaSb are solely a consequence of stabilization differences, then this result implies that one or both of these materials has growth kinetics for Sb_2 and Sb_4 that differ from the model proposed for As_2 and As_4 on GaAs [31,32].

In general, the ratios s_4/s_2 and g_4/g_2 need not be equal, because they relate to different processes. The value g_x involves Group V atoms that permanently incorporate into a growing crystal. There are frequent interactions between III and V species, and a large fraction of Group V species are buried by growth before they can desorb. The surface is highly disordered and has a high density of island edge sites. For (0 0 1) surfaces, g_x increases weakly with temperature under typical growth conditions [30], presumably as more Group V species desorb prior to incorporation. On the other hand, s_x relates to the replacement of Group V atoms that desorb from sites of the prevailing surface reconstruction and increases strongly with temperature (Figs. 3 and 4). The surface is flatter, more ordered, and has fewer types of adsorption sites. This strong distinction between stabilization and growth applies to those processes for AlSb and GaSb that are considered here.

For InAs, there is a weaker distinction between s_x and g_x, and a comparison is less meaningful. Here, both arsenic stabilization and arsenic-limited growth occur near the phase boundary between As- and In-rich reconstructions [(2×4) and (4×2)]. In fact, the arsenic flux corresponding to [$g_x \times$ (indium flux)] and the flux s_x plotted in Fig. 3 represent points on two different indium flux isobars (with finite and zero indium flux, respectively) of a single flux-temperature phase diagram for InAs growth. Ref. [23] discusses such phase diagrams for InAs. The comparison is complicated further by the fact that the InAs phase boundaries in Figs. 3 and 4 were obtained for temperatures considerably above where g_x was measured ($\sim$420°C). Measuring both growth and stabilization around 420°C is impractical, because extremely small arsenic fluxes would be needed for stabilization, while at higher temperatures (>500°C) the isobars merge, and the distinction between growth and stabilization is lost.

The slopes of the phase boundaries reflect kinetic differences in the ability of dimers and tetramers to stabilize the surface at the phase boundary. For a surface in equilibrium with vapor, the compositions of incident and desorbing fluxes would be equivalent, and the slope of a log pressure vs. inverse temperature plot is proportional to the free energy of desorption or adsorption. The situation

[6] Here we define efficiency as inversely proportional to the flux required for a given process. The stabilization flux s_x ranges from zero, where no Group V species desorb from the surface (and thus do not need replacing), to infinity, where no Group V species stick to the surface. The corresponding efficiency ranges from infinity to zero, respectively. The values g_x [Torr/(ML/s)] are proportional to the Group V flux required for V-limited growth, per unit of growth rate, and range from one (when Groups V and III atomic fluxes are equal) to infinity. The analogous efficiency ranges between one and zero, respectively.

[7] The ratios s_4/s_2 or g_4/g_2 by themselves are not meaningful numbers, because they contain unknown (and different) ionization efficiencies for dimers and tetramers. In the comparison $s_4/s_2 \leftrightarrow g_4/g_2$, however, the ionization efficiencies cancel out on left and right, so that we may compare the ratios for *stabilization* vs. *growth*.

in this work is better described as "steady state", because the incident Group V composition (dimer and tetramer concentrations) that is imposed by the experiment will generally not match the desorbing composition. In this case, the slopes and offsets of the reconstruction phase boundaries may depend on the energies and widths of various kinetic barriers. For InAs and AlSb, the two lines have different slopes, implying that the kinetics of dimer and tetramer incorporation are different. The parallel lines for GaSb suggest that there is a common rate-limiting incorporation step for dimers and tetramers. One possibility is that GaSb has only a small barrier for breakup of surface Sb_4 into dimers, so that dimer and tetramer kinetics are dominated by the barrier for subsequent dimer incorporation.

The adsorption of Group V species onto III–V surfaces is influenced by the surface structure and stoichiometry. Unlike the antimonides, InAs has a III-rich reconstruction on the high temperature side of the transition, so it is not surprising that the qualitative features of its phase boundaries are different than at least one of the antimonides. However, the similar dimer and tetramer phase boundary slopes for GaSb stand out compared to AlSb, considering that the two materials have similar surfaces. Above the phase transition, both exhibit a (4×3) bilayer-Sb reconstruction with a small fraction of Group III atoms ([40], see footnote 3). Below the phase transition, AlSb has a $c(4\times4)$ reconstruction, while GaSb shows (2×5)-like reconstructions. The (2×5) surfaces have the highest Group V content of any III–V zincblende material and are conducting rather than semiconducting [41]. These unusual features may contribute to the difference in AlSb and GaSb reactivity with the two types of antimony.

5. Conclusion

The surface reconstruction phase diagrams reported here should serve as a guide for optimizing growth conditions and as a means for calibrating substrate temperature for MBE growth of the 6.1 Å compound semiconductors. The phase boundaries for GaSb under dimer and tetramer antimony flux have similar slopes and little offset, in contrast to those for AlSb, suggesting fundamental differences in the kinetics of antimony stabilization of the two material surfaces.

Appendix

In order to apply the transmission thermometry technique to a given substrate material, a quantitative calibration curve is required. This curve gives the inflection point of the optical transmission spectrum as a function of the substrate temperature. Because the routinely used calibration curve [14] for GaAs substrates is known to be inaccurate by as much as 30°C, we present here updated calibration curves for semi-insulating and n^+-doped GaAs.

The technique used to obtain the calibration curves is described in detail in Ref. [16]. Briefly, a vacuum furnace was used to heat the GaAs substrate, and a spring-loaded thermocouple was placed in direct contact with the wafer. Transmission spectra were recorded for a series of substrate temperatures. In Fig. 5, the inflection point of the transmission edge is plotted as a function of substrate

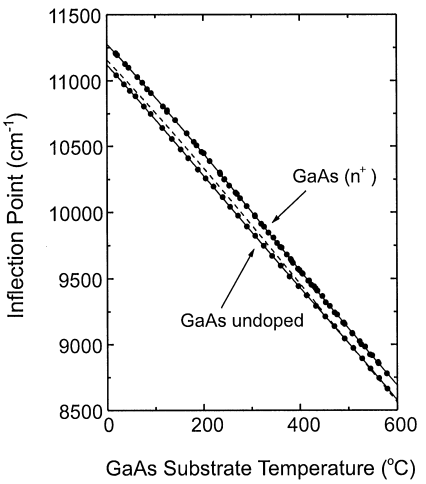

Fig. 5. Calibration curve for transmission thermometry of semi-insulating and n^+-doped ($n = 10^{18}\,cm^{-3}$) GaAs. The dashed curve represents the previous calibration from Ref. [14] for both types of substrates.

temperature. The fits are fourth-order polynomials with the form $T = a + bE + cE^2 + dE^3 + eE^4$, with T in °C and E in cm^{-1}. The coefficients are $a = -9070.5$, $b = 4.8124$, $c = -8.1385 \times 10^{-4}$, $d = 5.8157 \times 10^{-8}$, $e = -1.5514 \times 10^{-12}$ for semi-insulating GaAs and $a = -2.6712 \times 10^{4}$, $b = 11.759$, $c = -1.8343 \times 10^{-3}$, $d = 1.2436 \times 10^{-7}$, $e = -3.1536 \times 10^{-12}$ for n^+ GaAs. For these calibrations, wafer thickness was $470 \pm 15\,\mu m$ (SI–GaAs) and $440 \pm 15\,\mu m$ (n^+-GaAs). The n^+ doping level was $(1–1.5) \times 10^{18}\,cm^{-3}$.

Acknowledgements

The authors would like to thank B.V. Shanabrook for helpful discussions. This work was supported by the Office of Naval Research and DARPA under the Virtual Integrated Prototyping Initiative. ASB was supported by a National Research Council NRL Research Associateship.

References

[1] J.B. Boos et al., IEEE Trans. Electron. Devices 45 (1998) 1869.
[2] D.H. Chow et al., IEEE Electron. Device Lett. 17 (1996) 69.
[3] F. Fuchs et al., Appl. Phys. Lett. 71 (1997) 3252.
[4] W.W. Bewley et al., Appl. Phys. Lett. 74 (1999) 1075.
[5] P.R. Hammar et al., Phys. Rev. Lett. 83 (1999) 203.
[6] B.R. Bennett, B.V. Shanabrook, Molecular beam epitaxy of Sb-based semiconductors, in: A.W.K. Liu, M.B. Santos (Eds.), Thin Films: Heteroepitaxial Systems, World Scientific, London, 1999, p. 401.
[7] J.Y. Tsao, Materials fundamentals of Molecular Beam Epitaxy, Academic Press, Boston, 1993.
[8] M.A. Herman, H. Sitter, Molecular Beam Epitaxy: Fundamentals and Current Status, 2nd Edition, Springer, New York, 1996.
[9] T. Ito, K. Shiraishi, Jpn. J. Appl. Phys. 37 (1998) 4234.
[10] K. Shiraishi, Thin Sold Films 272 (1996) 345.
[11] B.V. Shanabrook, J.R. Waterman, J.L. Davis, R.J. Wagner, Appl. Phys. Lett. 61 (1992) 2338.
[12] B.V. Shanabrook, J.R. Waterman, J.L. Davis, R.J. Wagner, D.S. Katzer, J. Vac. Sci. Technol. B 11 (1993) 994.
[13] D.S. Katzer, B.V. Shanabrook, J. Vac. Sci. Technol. B 11 (1993) 1003.
[14] R. Powell, D. Kirillov, Improved temperature uniformity and measurements, in: T. Cooper (Ed.), Process and Technology Enhancements for MBE Production of MIMICS, MIMIC Phase III Contract DAAL01-89-C-0907, Varian Associates, Palo Alto, CA, 1991.
[15] E.S. Hellman, J.S. Harris, J. Crystal Growth 81 (1987) 39.
[16] M.J. Yang, W.J. Moore, C.H. Yang, R.A. Wilson, B.R. Bennett, B.V. Shanabrook, J. Appl. Phys. 85 (1999) 6632.
[17] J. Piao, R. Beresford, W.I. Wang, J. Vac. Sci. Technol. B 8 (1990) 276.
[18] M. Yano, H. Yokose, Y. Iwai, M. Inoue, J. Crystal Growth 111 (1991) 609.
[19] K. Reginski, J. Muszalski, V.V. Preobrazhenskii, D.I. Lubyshev, Thin Solid Films 267 (1995) 54.
[20] K. Reginski, J. Muszalski, V.V. Preobrazhenskii, D.I. Lubyshev, Thin Solid Films 267 (1995) 51.
[21] C. Chatillon, J.C. Harmand, F. Alexandre, J. Crystal Growth 130 (1993) 451.
[22] L. Däweritz, R. Hey, Surf. Sci. 236 (1990) 15.
[23] S.M. Newstead, R.A.A. Kubiak, E.H.C. Parker, J. Crystal Growth 81 (1987) 49.
[24] K. Yang, L.J. Schowalter, Appl. Phys. Lett. 60 (1992) 1851.
[25] A.M. Dabiran, P.I. Cohen, J. Crystal Growth 150 (1995) 23.
[26] H. Yamaguchi, Y. Horikoshi, Appl. Phys. Lett. 64 (1994) 2572.
[27] P.M. Thibado, B.R. Bennett, B.V. Shanabrook, L.J. Whitman, J. Crystal. Growth 175 (1997) 317.
[28] P.D. Brewer, D.H. Chow, R.H. Miles, J. Vac. Sci. Technol. B 14 (1996) 2335.
[29] E.S. Tok, J.H. Neave, F.E. Allegretti, J. Zhang, T.S. Jones, B.A. Joyce, Surf. Sci. 371 (1997) 277.
[30] E.S. Tok, T.S. Jones, J.H. Neave, J. Zhang, B.A. Joyce, Appl. Phys. Lett. 71 (1997) 3278.
[31] C.T. Foxon, B.A. Joyce, Surf. Sci. 50 (1975) 434.
[32] E.S. Tok, J.H. Neave, J. Zhang, B.A. Joyce, T.S. Jones, Surf. Sci. 374 (1997) 397.
[33] Y. Fukunishi, H. Nakatsuji, Surf. Sci. 316 (1994) 168.
[34] C.T. Foxon, B.A. Joyce, Surf. Sci. 64 (1977) 293.
[35] C.E.C. Wood, C.R. Stanley, G.W. Wicks, M.B. Esi, J. Appl. Phys. 54 (1983) 1868.
[36] C. Webb, D. Liu, J.N. Eckstein, Appl. Phys. Lett. 60 (1992) 571.
[37] A.K. Ott, S.M. Casey, S.R. Leone, J. Crystal Growth 181 (1997) 326.
[38] K.R. Evans, C.E. Stutz, P.W. Yu, C.R. Wie, J. Vac. Sci. Technol. B 8 (1990) 271.
[39] J.R. Waterman, B.V. Shanabrook, R.J. Wagner, J. Vac. Sci. Technol. B 10 (1992) 895.
[40] W. Barvosa-Carter, A.S. Bracker, B.R. Bennett, J.C. Culbertson, B.Z. Nosho, B.V. Shanabrook, L.J. Whitman, N. Modine, H. Kim, E. Kaxiras, Phys. Rev. Lett. 84 (2000) 4649.
[41] L.J. Whitman, P.M. Thibado, S.C. Erwin, B.R. Bennett, B.V. Shanabrook, Phys. Rev. Lett. 79 (1997) 693.